Physica B: Physics of Condensed Matter 530 (2018) 270–276

Contents lists available at ScienceDirect

Physica B: Physics of Condensed Matter

journal homepage: www.elsevier.com/locate/physb

Structural transition in Gd doped $LaCrO_3$ isovalent by in-situ ultrasonic measurements

P. Thamilmaran [a], M. Arunachalam [a], S. Sankarrajan [b], K. Sakthipandi [b,*], M. Sivabharathy [b], E. James Jebaseelan Samuel [c]

[a] Department of Physics, Sri SRNM College, Sattur 626 203, Tamil Nadu, India
[b] Department of Physics, Sethu Institute of Technology, Kariapatti 626 115, Tamil Nadu, India
[c] Department of Physics, School of Advanced Sciences, VIT University, Vellore 632 014, Tamil Nadu, India

ARTICLE INFO

Keywords:
Lanthanum chromite
Ultrasonic velocity
Attenuation
Structural transition

ABSTRACT

The Gadolinium substituted $LaCrO_3$ isovalent perovskite was investigated in the present study. The samples of $La_{1-x}Gd_xCrO_3$ ($x = 0$, 0.025, 0.05, 0.10, 0.15 and 0.20) were prepared employing solid state reaction method. The X-Ray Diffraction (XRD) patterns confirmed that the prepared samples have orthorhombic structure with pnma space group at room temperature. The crystalline size of the samples is 98, 89, 76, 72, 60 and 55 nm respectively for the composition x = 0, 0.025, 0.05, 0.10, 0.15 and 0.20 and the same is decreasing with an increase in substitution of Gd in the samples. The scanning electron microscope images of the samples have spherical like morphology with a particle size of 150, 131, 129, 120, 116 and 94 nm for the composition x = 0, 0.025, 0.05, 0.10, 0.15 and 0.20 respectively. In-situ ultrasonic measurements were made over a wide range of temperature from 300 to 700 K to determine structural transition. The measured temperature dependent ultrasonic parameters are used to explore the structural phase transition from orthorhombic to rhombohedral phase in the prepared sample at high temperatures.

1. Introduction

The rare earth orthochromites $RCrO_3$ (R-La, Pr, Nd) have attracted many researchers because of their unique structural, electrical and magnetic properties [1–3]. If R ion is magnetic, there are interactions such as Cr^{3+}—Cr^{3+}, R^{3+}—Cr^{3+}, R^{3+}—R^{3+} causes a complex magnetic behaviour [1]. If R is non-magnetic ion, then Cr—O—Cr super exchange interaction with antiferromagnetic (AFM) order takes place. This is due to Dzyaloshinsky-Moriya (DM) exchange interaction between neighbouring spins. The interaction induced by temperature or by an applied magnetic field between R^{3+} and Cr^{3+} resulting a spin reorientation, antisymmetric and anisotropic symmetric exchange interaction [2,3].

The lanthanum chromite perovskite oxides exhibit two types of phase transitions. The first one is at low temperature phase transition due to magnetic order – disorder transition from an AFM to paramagnetic (PM) state below 300 K [4,5]. This low temperature AFM order is governed by Cr—O—Cr super exchange interaction. This results in the Cr sub-lattices with a canting of spins at Cr site below Neel temperature (T_N) ≃300 K, attributed to asymmetric exchange interaction between neighbouring spins [6]. The static magnetic susceptibility [7], electron paramagnetic resonance [8], adiabatic calorimetry [9] and neutron diffraction [10] studies were carried out to ascertain the low temperature AFM to PM phase transition. The other one is the structural transition i.e., from orthorhombic to rhombohedral phase taking place at high temperatures is accompanied by volume shrinkage and the buckling and tilting of CrO_6 octahedral. The high temperature structural transition in the perovskites is reported using differential scanning calorimetry (DSC) [11], thermal gravity-DSC with X-ray diffraction (XRD) [12].

The $LaCrO_3$ orthochromite has an AFM order with Cr^{3+} moments aligning in canted orientation [6,13]. The doping of divalent ion such as Ba, Ca, Sr, on $LaCrO_3$ was studied to evaluate the structural and magnetic properties. $La_{1-x}Ca_xCrO_3$ perovskite showed a decrease in T_N substantially with increasing calcium doping concentration (x = 0 to 0.3) from 290 K to 160 K. The Ca substitution for La site causes shrinkage of all the three cell parameters and volume of unit cell. The increase in Ca content causes a shift in arrangement of CrO_6 octahedrons in the structure. The Cr—O—Cr angles become larger with increase in Ca content [13]. Similar investigations [14–16] was made on Ca doped $LaMnO_3$ perovskite samples to study metal-insulator transition and ferromagnetic (FM) to PM transitions. The structural transition from orthorhombic to

* Corresponding author.
E-mail address: sakthipandi@gmail.com (K. Sakthipandi).

https://doi.org/10.1016/j.physb.2017.11.073
Received 21 September 2017; Received in revised form 1 November 2017; Accepted 25 November 2017
Available online 2 December 2017

rhombohedral structure was observed about 600 K in calcium doped $LaCrO_3$ orthochromite [17].

The two different types of doping are used to obtain the La-site modification in doped perovskites ($LaCrO_3$). The first one is the substitution of La-site with different valence elements which is known as carrier doping. The other is the modification of ionic radius wherein La-site is substituted with ions having the same valence but different ionic radius. The averaged radius of lanthanum and substituted ions affects bond length and bond angle of Cr—O—Cr. Hence, it leads to a change of effective transfer energies between Cr sites. The magnetic properties of $GdCrO_3$ perovskite nanoparticles exhibit spin reorientation with AFM transition at 168 K which is in agreement with the reported value of 167 K for samples [18] inferring that the size of the particles does not affect the transition temperature [19]. While doping isovalent elements, DE interaction cannot play any role and spin canting results from DM [20] interaction leads to a canted AFM spin state persists at low temperatures [21]. The doping of Gd^{3+} for La^{3+} gives raise the interaction between Cr—Gd which shows a spontaneous spin reorientation of the Cr system. This change in average ionic radius leads to the structural transition, lattice deformation and rotation in CrO_6 octahedral [20,21].

The XRD studies on the undoped $LaCrO_3$ sample show an orthorhombic structure whereas the Mn half doped sample exhibits rhombohedral structure. This indicates that the substitution of Mn^{3+} causes the structural transition [22]. The investigation on $La_{1-x}Pr_xCrO_3$ ($0 \leq x \leq 1$) perovskites showed an orthorhombic phase in the entire composition region at room temperature. The studies on the magnetic properties of these samples exhibit AFM phase at 288 K for $LaCrO_3$ ($x = 0$) and 240 K for $PrCrO_3$ ($x = 1$). The value of T_N decreases with the increasing value of x. It is attributed to the continuous change of a Cr^{3+}—O^{2-}—Cr^{3+} angle governing the AFM interaction between Cr^{3+}. This is due to the same type of magnetic interaction as in an isostructural compound [23]. Neha Sharma et al. studied the magnetic behaviour of $La_{1-x}Gd_xCrO_3$ ($x = 0.5$ and 0.9). The samples showed a canted AFM order and the observed T_N values are 225 K for $x = 0.5$ and 177 for $x = 0.9$ [24,25]. Hence, the result indicates that an increase in Gd content in the sample leads to a decrease in T_N.

The structural and phase transition of the perovskites were studied employing different techniques such as XRD, neutron diffraction etc. [7–10]. Ultrasonic characterisation is a versatile and sensitive tool to explore the structural/phase transition and also to obtain the elastic properties. The temperature dependence of ultrasonic measurements of longitudinal, shear velocities and its attenuation was used to detect the phase transition temperatures such as Curie temperature (T_c), Jahn-Teller temperature (T_{JT}), metal insulator transition temperature (T_{MI}) etc., and structural transition [26,27]. Further, the use of temperature dependent ultrasonic measurements to study the structural transition is easy and economical compared to other techniques.

The various synthesis techniques [28] have been proposed and developed to prepare the perovskites over the years. The choice of a particular one basically depends on various factors such as the availability, reaction time, cost, and expected morphology. The three factors such as degree of crystallinity, chemical composition and crystal morphology of perovskites (i.e., particle sizes, pore size distribution and specific surface area) were affected by the synthesis techniques and the specific synthesis conditions [29]. Among these techniques, the solid-state reaction is mostly used to prepare the whole range of materials including mixed perovskites, metal oxides, sulphides, nitrates and alumina silicate. The advantages of using the solid state reaction are simple to perform, direct reactions among the starting materials and economical [30].

In the survey of literature, no structural transition study on $LaCrO_3$ perovskite with isovalent doping was reported so far. Huseo et al. observed that in the sample $(La_{1-x}Gd_x)_{0.67}Ca_{0.33}MnO_3$, the value of T_c drops from 260 K for the undoped sample to 100 K for the doping of Gd by 25% [31]. The decline in the value of T_c is ascribed to the structural changes. In the present work, $La_{1-x}Gd_xCrO_3$ isovalent perovskite samples with different composition of $x = 0.0$, 0.025, 0.05, 0.10, 0.15 and 0.20 were synthesized. The structure, morphology and the properties of the samples were studied using XRD, scanning electron microscope (SEM) and ultrasonic characterisation techniques. The temperature dependent in-situ measurement of ultrasonic parameters was made over a wide range of temperature from 300 to 700 K. The obtained results were analyzed and correlated with the structural transition on the Gd doped $LaCrO_3$ orthochromite samples.

2. Materials and methods

2.1. Preparation of $La_{1-x}Gd_xCrO_3$ isovalent perovskite

$La_{1-x}Gd_xCrO_3$ ($x = 0$, 0.025, 0.05, 0.10, 0.15 and 0.20) isovalent perovskite samples were prepared employing solid state reaction [15,16] technique by taking stoichiometric quantity of pure grade La_2O_3, Cr_2O_3 and Gd_2O_3 as starting materials having purity 99.9%. The stoichiometric amount of powders required for the sample preparation were weighed using digital balance (ATX224, Shimadzu, Japan) and were well mixed in an agate mortar and ground finely. The mixture was calcined at 873 K for 2 h and then ground to obtain a homogeneous mixture. Once again, the mixture was calcined at 873 K for 2 h after the fine grinding. Then, the calcined mixture was pressed into pellets of thickness of 3 mm and diameter of 12 mm using a stainless steel dye. The pressed pellets were sintered at 1273 K for 12 h and then, cooled to room temperature. These sintered pellets were used for further investigation. Hereafter, the samples are called as LGCO000, LGCO025, LGCO050, LGCO100, LGCO150 and LGCO200 respectively for the composition x = 0, 0.025, 0.05, 0.10, 0.15 and 0.20.

2.2. Characterisation of $La_{1-x}Gd_xCrO_3$ isovalent perovskite

The crystalline nature of the prepared sample was obtained using a powder X-ray diffractometer (X'Pert Pro, PANalytical, the Netherlands) using CuK_α radiation source ($\lambda = 1.5406\ A^0$). By using Fullprof software technique, the structural parameters of the samples were examined by Rietveld analysis of the obtained XRD data. The microstructure and morphology of the prepared samples were studied using SEM (JOEL, JED5300, Japan). The density of the samples was measured employing Archimedes principle using CCl_4 as buoyant. The density of the sample was calculated by using the standard relation [32].

A high power ultrasonic pulse receiver with a fundamental frequency 5 MHz (Olympus NDT, 5900 PR, USA) was used to carry out the measurement of ultrasonic velocity and attenuation in both longitudinal and shear mode over a wide range of temperature 300–700 K. A 1 GHz digital storage oscilloscope (DSO) (Lecroy, wave runner 104 Mxi, USA) was used to record the digital RF ultrasonic signals. The longitudinal and shear ultrasonic waves were generated at a fundamental frequency of 5 MHz using X-cut and Y-cut transducers respectively. The temperature of the sample region was controlled using a programmable temperature controller (Eurotherm, 2604, USA) at a heating rate of 0.5 K min^{-1}. The accuracy in the measurement of velocity is ±2 m s^{-1} and that of temperature is ±1 K. The temperature dependent measurements of ultrasonic parameters were carried out using through transmission technique as discussed in the early studies [26]. The measured density (ρ) and longitudinal (U_L) and shear (U_S) velocities were used to obtain the elastic moduli such as longitudinal (L), shear (G), bulk (K) and Young's (E) modulus using standard equations [32].

3. Result and discussion

The XRD pattern of $La_{1-x}Gd_xCrO_3$ isovalent perovskite samples is shown in the Fig. 1. The observed diffracted peak at planes (101), (121), (022), (202), (222), (042), (242), (420) and (323) in LGCO000 confirms the orthorhombic structure with *Pnma* space group at room temperature. (JCPDS File No. 89-8770) [33,34]. Further, the XRD patterns of

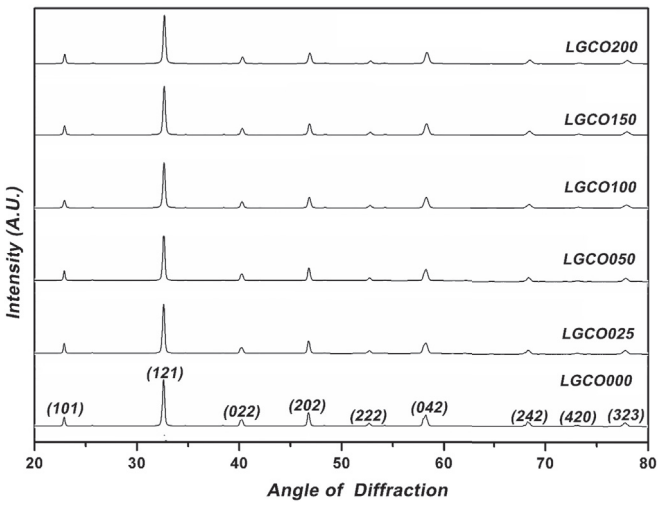

Fig. 1. XRD pattern of LGCO samples.

LGCO025, LGCO050, LGCO100, LGCO150 and LGCO200 samples also exhibit the similar peak positions at the same diffracted planes. It is evident that the substitution of Gd in $LaCrO_3$does not alter the XRD diffracted planes. Similar studies carried out on LGCO samples with the substitution of Gd reveal the same XRD patterns [23–25]. The increase in Gd content causes a decrease in unit cell volume. It is attributed to the decrease in average ionic radius caused by the smaller ionic radius of the Gd content (1.27 A^0) than that of La (1.36 A^0). This is due to the increase in distortion of the isovalent perovskite structure observed through decreasing Cr—O—Cr bond angles [35].

The obtained Goldschmidt's tolerance factor [33] of the samples was calculated, the lattice parameters of the samples and the average crystalline size of the sample obtained using Scherrer's equation [32] are listed in Table 1. The lattice parameters and the volume of the unit cell decrease with the increase in doping level of Gd in the prepared $La_{1-x}Gd_xCrO_3$ isovalent perovskite samples. The decrease in Goldschmidt's tolerance factor with the increase in the doping level of Gd content indicates the expected distortion in the isovalent perovskite structure [35]. From Table 1, it is seen that greater distortion occurs as the Gd content becomes more.

The SEM images (Fig. 2) of the LGCO samples indicate the formation of cluster and agglomeration of the particle with spherical like morphology. The average size of the particle obtained by calculating the mean diameter of number of particles is 150, 131, 129, 120, 116 and 94 nm for the samples LGCO000, LGCO025, LGCO050, LGCO100, LGCO150 and LGCO200 respectively. It reveals that the substitution of Gd^{3+} on La^{3+} sites in $LaCrO_3$ samples affects the agglomerate size. The average agglomerate size of the particles gradually decreases with the increase in the composition of Gd in the material which is attributed to the decrease in mean ionic radius caused by the addition of doping material [36,37]. Ionic radius of the Gd^{3+} (1.27 Å) is smaller than that of La^{3+} (1.36 Å). Hence, it creates compaction stress in structure [38,39]. Therefore, Gd^{3+} with lower radius may suppress the formation of larger nuclei during the crystallization process. Hence, the particle size is reduced with an increase in Gd content. The mean diameter of La^{3+} and Gd^{3+} decreases with an increase in Gd content in the sample. The reason for the reduction of grain size is due to physiochemical effect [40]. During the sintering of compound the smaller radius ion (Gd) will partially enter into the lattice and the remaining will diffuse to the grain boundaries which lead to an isolated thin layer around the crystallites. Hence, the stress is introduced in the crystal when Gd ions get into the lattice. The accumulated Gd ions at the grain boundary act as a kinetic barrier for further grain displacement. Thus, a hinder in the grain growth occurred in the samples [41]. The decrease in grain size with increasing Gd concentration in $Zn_{1-x}Gd_xO$ [41] and $(Bi_{1-x}Gd_x)_{0.5}Na_{0.5}TiO_3$ [42] was reported.

Table 1
Lattice parameters, volume of unit cell and crystalline size and tolerance factor of LGCO samples.

Sample	a (A^0)	b (A^0)	c (A^0)	Unit cell volume $(A^0)^3$	Crystallite size (nm)	Tolerance factor
LGCO000	5.478	7.759	5.515	234.46	98	0.9147
LGCO025	5.477	7.757	5.514	234.31	89	0.9139
LGCO005	5.477	7.753	5.508	233.93	76	0.9131
LGCO100	5.476	7.746	5.501	233.40	72	0.9116
LGCO150	5.475	7.743	5.497	233.05	60	0.9099
LGCO200	5.481	7.748	5.473	232.66	55	0.9085

The observed density values of the prepared samples at the room temperature are 5972, 6094, 6208, 6347, 6471 and 6522 kg m^{-3} for the samples LGCO000, LGCO025, LGCO050, LGCO100, LGCO150 and LGCO200 respectively. It is noticed that the density of the samples increases as the content of Gd^{3+} increases. The increase in density occurs due to the close packing of the structure that caused by the decrease in distortion [16]. Generally, the decrease in distortion leads to decrease in lattice of the unit cell. Hence, the volume of the unit cell is decreased which in turn increases the density [43]. Density depends on the effective number of atoms in a unit cell and orientation of packing of atoms within the unit cell. The increase in Gd^{3+} concentration leads to closed pack structure. Therefore, the increase in density may be correlated with a decrease in distortion that caused by the close packing of the structure. However, the increase in density also depends on density of the constitution elements. Density of the sample increases due to the Gd (7895 kg m^{-3}) has large density compared to the La (6162 Kgm^{-3}). The necessary discussion is incorporated in the revised manuscript.

The ultrasonic parameters such as longitudinal velocity (U_L), shear velocity (U_S), longitudinal attenuation (α_L), shear attenuation (α_S) and elastic constants of the prepared LGCO samples measured at the room temperature are listed in Table 2. It is to be noted that ultrasonic velocities (U_L and U_S) decrease with the increase in Gd content in the samples. The elastic constants also showed a similar observation as that of velocities [15,16]. The ultrasonic velocity as a function of temperature is used to obtain the information about the structure/phase transition and its behaviour [26,32]. The temperature dependent U_L and U_S are respectively shown in Table 3 and Figs. 3 and 4.

In order to understand the temperature dependent behaviour of the ultrasonic parameters on the prepared chromite samples, the entire range of temperatures is divided into three different zones. For the sample LGCO000, Zone I starts from 300 and ends at 526 K, the temperature at which the anomalous behaviour starts. Zone II is the anomalous region that lies between 526 and 536 K at which the anomalous behaviour ends and Zone III is from 536 to 700 K. It is revealed from Fig. 3 that U_L shows a monotonic decrease as a function of temperature both in Zone I and in Zone III. This indicates the absence of structural transition in Zone I and II. However, an anomalous behaviour is observed in Zone II. Up to the beginning of Zone II, there is a smooth decrease in longitudinal velocity from 6154 to 5470 m s^{-1}. The decline in velocity is so abrupt from 526 to 532 K with the velocity 5470 and 5285 m s^{-1} respectively followed by a sharp increase up to 536 K with a longitudinal velocity 5350 m s^{-1}. Thereafter up to 700 K, once again the sample shows a smooth decrease in velocity with 4469 m s^{-1} in Zone III. In Zone II, the temperature at which the velocity is minimum at 532 K and is called the anomalous temperature. The temperature dependence of U_S (Fig. 4) also shows a similar trend whereas a reverse behaviour is observed in the case of longitudinal (α_L) and shear (α_S) attenuation (Figs. 5 and 6). Instead of a dip, a sharp peak is observed in the anomalous zone in the case of α_L and α_S. Similarly, the anomalous temperature for the samples LGCO025, LGCO050, LGCO100, LGCO150 and LGCO200 are 524, 508, 484, 456 and 422 K respectively.

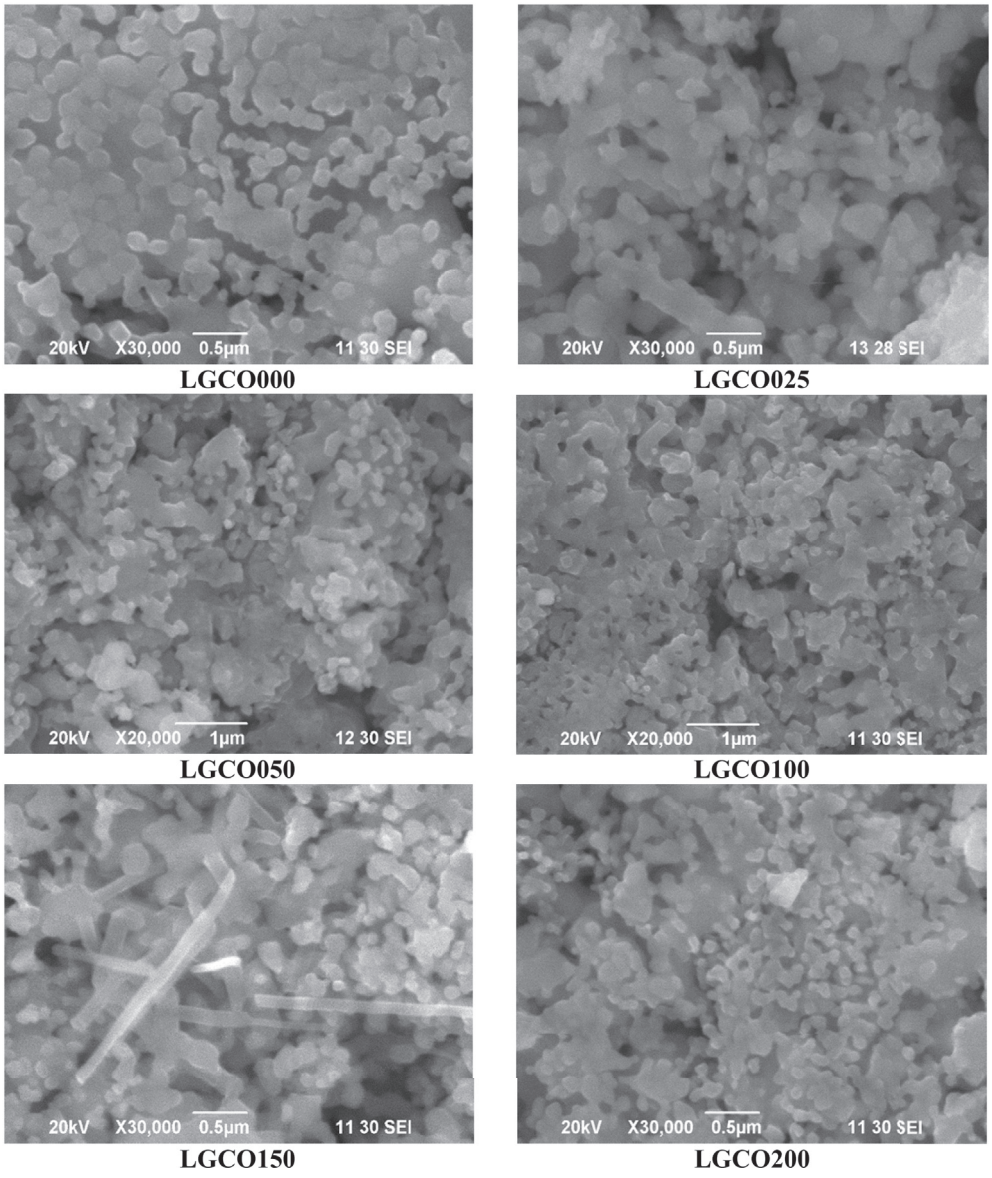

Fig. 2. SEM images of LGCO samples.

Table 2
Density and ultrasonic parameters of LGCO samples at 300 K.

Parameters	LGCO000	LGCO025	LGCO050	LGCO100	LGCO150	LGCO200
Density (Kgm^{-3})	5972	6094	6208	6347	6471	6522
U_L (ms^{-1})	6154	5931	5509	5159	4947	4583
U_S (ms^{-1})	3127	3002	2795	2611	2504	2318
α_L ($dBcm^{-1}$)	1.431	1.64	1.9228	2.135	2.376	2.521
α_S ($dBcm^{-1}$)	5.7632	6.172	6.864	7.218	7.681	8.101
L (G Pa)	226.200	214.377	188.401	168.91	158.37	136.99
G (G Pa)	58.4251	54.9232	48.5042	43.26	40.58	35.06
K (G Pa)	148.320	141.165	123.745	111.24	104.27	90.26
E (G Pa)	154.929	145.644	128.805	114.90	107.76	93.12

The observed anomalous temperatures in the prepared LGCO samples can be correlated with the structural transition from orthorhombic to rhombohedral. At this point, it would be appropriate to mention such an anomalous zone obtained in the undoped LGCO000 sample in the temperature from 526 to 536 K with the anomalous temperature 532 K. This temperature corresponds to the orthorhombic to rhombohedral structural transition obtained in various studies [44–46]. Further, from the above observations, it is inferred that the anomalous temperature decreases as the doping content Gd increases in the LGCO samples.

Neutron diffraction studies carried out by Oikawa et al. on $LaCrO_3$ orthochromite revealed a phase transition from orthorhombic to rhombohedral around 533 K [44]. They attributed the structural transition to the decrease in lattice parameters and volume compression of the unit cell which is caused by the shrinkage of the CrO_6 octahedral. It is to be noted that the structural transition temperature (T_S) is in close agreement with the observation made in the present investigation.

Table 3
Anomalous zone of temperature dependence of U_L in LGCO perovskite samples.

Sample	Start	Anomaly	End	Range
LGCO000	526	532	536	10
LGCO025	518	524	530	12
LGCO050	500	508	516	16
LGCO100	472	484	490	18
LGCO150	442	456	462	20
LGCO200	408	422	434	26

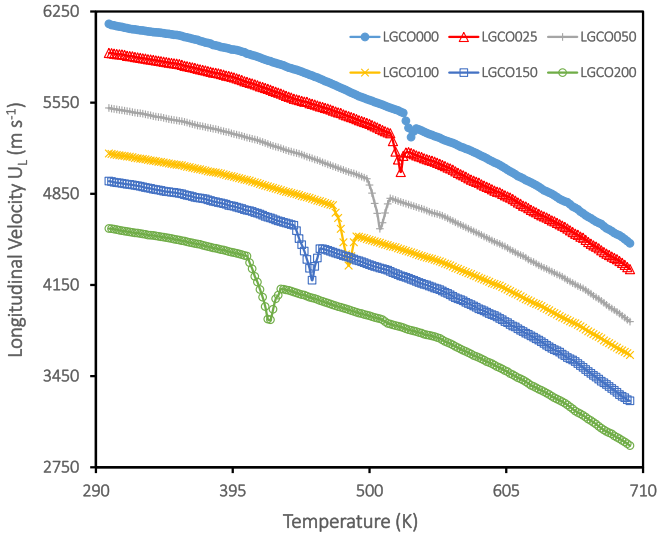

Fig. 3. Temperature dependence of longitudinal velocity of LGCO samples.

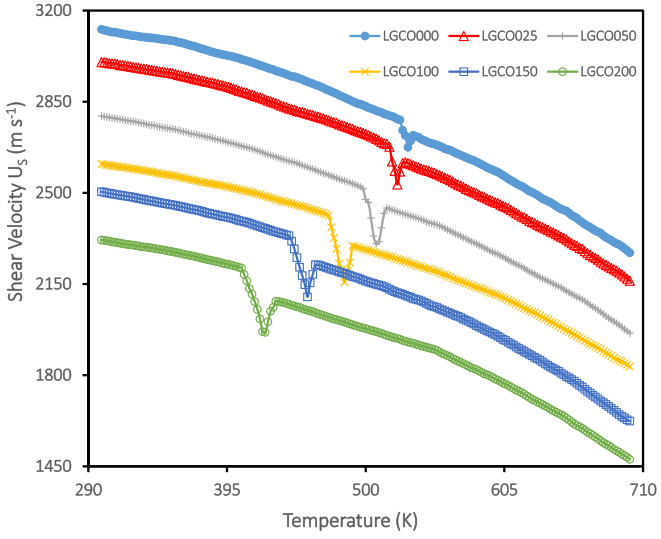

Fig. 4. Temperature dependence of shear velocity of LGCO samples.

Structural transition studies made on $LaCrO_3$ by the simultaneous measurement of DSC-XRD indicated that the phase transition from orthorhombic to rhombohedral with discrete volume compression. The transition started at 523 K and was completed at 541 K and there is no intermediate phase other than these two was reported [45]. It is worthy to note the temperature range of structural transition is so precise (from 526 to 536 K) in the present investigation. The observed anomaly in the temperature dependent measurement of thermal expansion coefficient on $LaCrO_3$, in the temperature range from 100 to 873 K revealed the orthorhombic to rhombohedral structural phase transition around 530 K

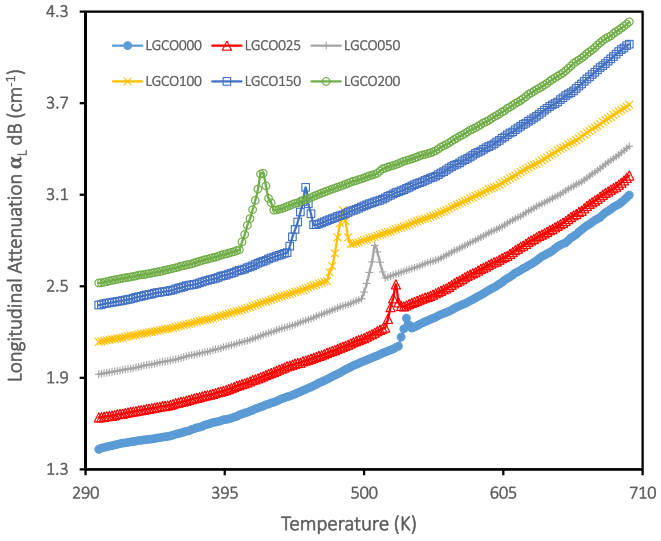

Fig. 5. Temperature dependence of longitudinal attenuation of LGCO samples.

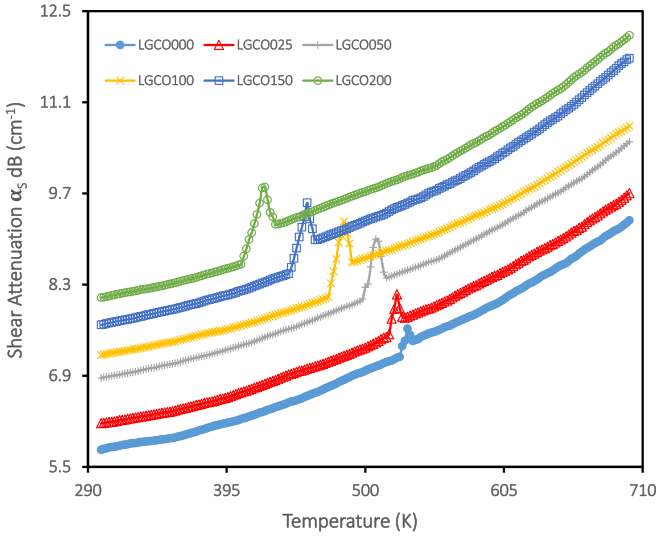

Fig. 6. Temperature dependence of shear attenuation of LGCO samples.

due to the volume shrinkage [46].

The doping of Gd^{3+} in the La site causes the reduction of tolerance factor as a consequence of the decrease in mean ionic radii and the decrease in mean bond length [17]. These changes in samples are primarily responsible for the reduction in the structural transition temperature [47]. Hence, the discussion leads to the conclusion that the observed anomalous temperatures in the ultrasonic studies, 532, 524, 508, 484, 456 and 422 K for the respective samples LGCO000, LGCO025 LGCO050, LGCO100, LGCO150 and LGCO200 are the structural transition temperature (T_S) from orthorhombic to rhombohedral structure.

Further for Better understanding, the tolerance factor for each composition is compared with its corresponding structural transition temperature. Fig. 7 shows the comparison of tolerance factor and structural transition temperature. It is evident from Fig. 7 that both the tolerance factor as well as the structural transition temperature decreases with the increase of gadolinium content in the sample. It is attributed to the octahedral tilting caused by the doping of Gd with smaller ionic radius which results in a structural transition [47]. From the temperature dependent ultrasonic velocities shown in Figs. 3 and 4, it is evident that the area of anomalous region becomes wider with the level doping content of gadolinium. The observed variation in ultrasonic velocities (U_L

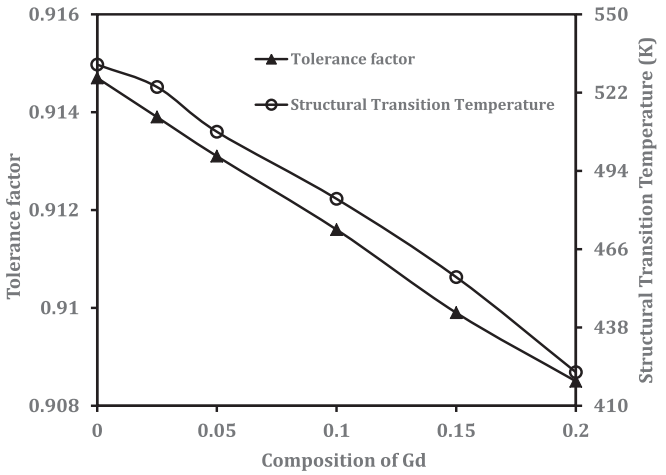

Fig. 7. Comparison between the Tolerance factor and Structural Transition Temperature.

and U_S) is correlated to the lattice volume fluctuations around the structural phase transition [48]. This also causes a sudden change of the orthorhombic lattice parameters or Cr—O bond length [48]. Hence, a competition between orthorhombic and rhombohedral structures comes to exist in the samples.

4. Conclusion

$La_{1-x}Gd_xCrO_3$ (x = 0.0, 0.025, 0.05.0.10, 0.15 and 0.20) isovalent perovskite samples were synthesized by solid state reaction route. The crystalline nature of the samples was confirmed by the XRD patterns. The samples have orthorhombic structure with pnma space group. The crystalline size of the samples decreases from 98 to 55 nm when the level of gadolinium increases from 0 to 20%. The size of the particles determined using the SEM images also behave in the same fashion like XRD. It ranges from 150 to 94 nm. In-situ measurement of ultrasonic velocities and attenuation carried out on the LGCO chromite samples over a wide range of temperatures. It shows an anomaly at the structural phase transition temperature (T_S). The value of T_S are 532 (x = 0.000), 524 (x = 0.025), 508 (x = 0.050), 484 (x = 0.100), 456 (x = 0.150) and 422 (x = 0.200) K indicating a decrease in T_S with the increase in doping concentration of Gd^{3+} brings the rhombohedral structure from the orthorhombic structure.

Acknowledgements

One of the authors (K.S) is thankful to Science and Engineering Research Board (SERB), New Delhi (Sanction no.: SR/FTP/PS-068/2014) for the financial support.

References

[1] T. Yamaguchi, Theory of spin reorientation in rare earth orthochromites and ortho ferrites, J. Phys. Chem. Solids 35 (1974) 479–500.
[2] K.B. Aring, A.J. Sievers, Role of the Ytterbium spins in the spin reorientation in $YbFeO_3$, J. Appl. Phys. 41 (1970) 1197.
[3] T. Sakata, A. Enomura, Studies of the rare earth ion interactions in the orthoferrites $GdFeO_3$ and $HoFeO_3$, Phys. Stat. solidi A 52 (1979) 311–314.
[4] C.P. Khattak, D.E. Cox, Structural studies of the (La, Sr) CrO_3 system, Mat. Res. Bul. 12 (1977) 463–471.
[5] A.H. Cooke, D.M. Martin, M.R. Wells, Magnetic interaction in gadolinium orthochromite, $GdCrO_3$, J. Phys. C. Solid. Stat. Phys. 7 (1974) 3133–3144.
[6] V.A. Khomchenko, I.O. Troyanchuck, R. Syamczak, H. Syamczak, Negative magnetization in $La_{0.75}Nd_{0.25}CrO_3$ perovskite, J. Mater. Sci. 43 (2008) 5662–5665.
[7] K.P. Bansal, S. Kumari, B.K. Das, G.C. Jain, On Some Transport properties of Strontium doped lanthanum chromite ceramics, J. Mater. Sci. 18 (1983) 2095–2100.
[8] I. Weinberg, P. Larssen, Electron paramagnetic resonance and antiferromagnetism in $LaCrO_3$, Nature 192 (1961) 445–446.
[9] N. Sakai, S. Stolen, Heat capacity and thermodynamic properties of lanthanum (III) chromite (III): LaCrO3 at temperatures from 298.15 K. Evaluation thermal conductivity, J. Chem. Thermodyn. 27 (1995) 493–506.
[10] W.C. Koehler, E.O. Wollan, Neutron-diffraction study of magnetic properties of perovskites-like compounds, $LaBO_3$, J. Phys. Chem. Solids 2 (1957) 100–106.
[11] T. Hashimoto, Pressure induced structural phase transition of $LaCrO_3$, Sol. Stat. Comm. 108 (1998) 691–694.
[12] Q. Shu, J. Zhang, J. Liu, The phase transition of O-orthorhombic $LaMn_{0.95}O_{3.02}$ at high temperature, J. Alloy. Comp. 461 (2008) 481–485.
[13] G.A. Alvarez, X.L. Wang, G. Peleckis, S.X. Dou, J.G. Zhu, Z.W. Lin, Magnetotransport and magnetic properties of weak ferromagnetic semiconductors: Ca doped LaCrO3, J. Appl. Phys. 103 (2008) 1–3, 07B916.
[14] K.P. Ong, P. Wu, L. Liu, S.P. Jiang, Optimization of electrical conductivity of $LaCrO_3$ through doping: a combined study of molecular modeling and experiment, Appl. Phys. Lett. 90 (2007) 04419.
[15] M. Arunachalam, P. Thamilmaran, S. Sankarrajan, K. Sakthipandi, Study of high temperature metal-insulator phase transition in $La_{1-x}Ca_xMnO_3$ employing ultrasonic studies, Phys. B Cond. Matter 456 (2015) 118–124.
[16] P. Thamilmaran, M. Arunachalam, S. Sankarrajan, K. Sakthipandi, On-line ultrasonic characterisation of barium doped lanthanum perovskites, Phys. B Cond. Matter 466 (2015) 19–25.
[17] N. Sakai, H. Fjellveg, B.C. Hauback, Structural, magnetic and thermal properties of $La_{1-t}Ca_tCrO_{3-\delta}$, J. Sol. Stat. Chem. 121 (1996) 202–213.
[18] B. Rajeswaran, D.I. Khomski, A.K. Zvezdin, C.N.R. Rao, A. Sundaresan, Field induced polar order at the Neel temperature of chromium in rare earth orthochromites: interpaly of rare earth and Cr magnetism, Phys. Rev. B 86 (2012), 214409.
[19] Y. Sundarayya and S. Srinath, Synthesis and magnetic properties of ferroelectric $GdCrO_3$ nanoparticles, Condens. Matter, Mesoscale Nanoscale Phys., 1402, arXiv: 1402.4260
[20] I. Solovyev, N. Hamada, K. Terakura, Crucial role of lattice distortion in the magnetism of $LaMnO_3$, Phys. Rev. Lett. 76 (1996) 4825–4828.
[21] V. Skumryev, F. Ott, J.M.D. Coey, A. Anane, J.P. Renard, L. Pinsart – Gaudart, A. Revcolevschi, Weak ferromagnetism in $LaMnO_3$, Eur. Phys. J.B 11 (1999) 401–406.
[22] P. Barrozo, J. Albino Agiur, Ferro magnetism in Mn half doped $LaCrO_3$ perovskite, J. Appl. Phys. 113 (2013), 17E309:1–3.
[23] K. Yoshi, A. Nakamura, Y. Ishii, Y. Morii, Magnetic properties of $La_{1-x}Pr_xCrO_3$, J. Solid State Chem. 162 (2001) 84–89.
[24] Neha Sharma, Bipin K. Srivatsava, Anjali Krishnamoorthi, A.K. Nigam, Magnetic behaviour of orthochromite $La_{0.5}Gd_{0.5}CrO_3$, Solid State Sci. 12 (2010) 1464–1468.
[25] Neha Sharma, Bipin K. Srivatsava, Anjali Krishnamoorthi, A.K. Nigam, Hysterisis in magnetization – temperature curves of orthochromite$La_{0.1}Gd_{0.9}CrO_3$, J. Alloys. Compd. 545 (2012) 50–52.
[26] P. Thamilmaran, M. Arunachalam, S. Sankarrajan, K. Sakthipandi, Impact of Ni doping on $La_{0.7}Sr_{0.3}Ni_xMn_{1-x}O_3$Perovskite manganite materials, J. Magn. Magn. Mater. 396 (2015) 181–189.
[27] K. Sakthipandi, V. Rajendran, On-line phase transition of bulk and nanocrystalline $La_{1-x}Pb_xMnO_3$(x=0.3, 0.4 and 0.5) perovskite manganite materials using ultrasonic measurements, Mat. Chem. Phys. 138 (2013) 586–592.
[28] K. Sakthipandi, V. Rajendran, T. Jayakumar, Baldev Raj and P. Kulandivelu, Synthesis and on-line ultrasonic characterisation of bulk and nanocrystalline $La_{0.68}Sr_{0.32}MnO_3$ perovskite manganite, J. Alloys. Compd. 509(8), 3457–3467.
[29] M.S. Shojai, M.T. Khorasani, Ehsan Dinpanah-Khoshdargi, Ahmad Jamshidi, Synthesis methods for nanosized hydroxyapatite with diverse structures, Acta Biomater. 9 (8) (2013) 7591–7621.
[30] M.H. Sarvari, H. Sharghi, Reactions on a solid surface: a simple, economical and efficient Friedel−Crafts acylation reaction over zinc oxide as a New catalyst, J. Org. Chem. 69 (20) (2004) 6953–6956.
[31] E. Hueso, J. Rivas, P. Sande, A. Fondado, F. Rivadulla, M.A. Lopez-Quintela, Effect of the progressive substitution of La^{3+} by Gd^{3+} in the magnetic and transport properties of $La_{2/3}Ca_{2/3}MnO_3$, J. Magn. Magn. Mater. 235 (2002) 293–300.
[32] P. Kulandaivelu, K. Sakthipandi, P. Senthilkumar, V. Rajendran, Mechanical properties of bulk and nano structured $La_{0.61}Sr_{039}MnO_3$ perovskite manganite materials, J. Phys. Chem. Solids 74 (2013) 205–214.
[33] H. Taguchi, S. Ichiro, M. Nagao, H. Kido, Electrical properties of perovskite type $La(Cr_{1-x}Mn_xO_{3-\delta})$, Phys. B Cond. Matt. 270 (1999) 325–331.
[34] V.D. Nithya a, R. Jacob Immanuel a, S.T. Senthilkumar a, C. Sanjeeviraja b, I. Perelshtein c, D. Zitoun c, R. Kalai Selvan, Studies on the structural, electrical and magnetic properties of LaCrO3, $LaCr_{0.5}Cu_{0.5}O_3$ and $LaCr_{0.5}Fe_{0.5}O_3$ by sol–gel method, Mater. Res. Bull. 47 (2012) 1861–1868.
[35] L.M. Daniels, M.D. Weber, M.R. Lees, M. Guennou, R.J. Kashtiban, J. Sloan, J. Kreisel, R.I. Walton, Structures and magnetism of the rare-earth orthochromite perovskite solid solution $laxsm_{1-x}cro_3$, Inorg. Chem. 52 (20) (2013) 12161–12169.
[36] S.P. Jiang, L. Liu, K.P. Ong, P. Wu, J. Li, J. Pu, Electrical conductivity and performance of doped $LaCrO_3$ perovskite oxides for solid oxide fuel cells, J. Power Sources 176 (2008) 82–89.
[37] M.K. Anupama, B. Rudraswamy, Effect of Gd3+- Cr3+ ion substitution on the structural, electrical and magnetic properties of Ni- Zn ferrite nanoparticles, IOP Conf. Series, Mater. Sci. Engg 149 (2016), 012194.
[38] Imran Sadiq, Imran Khan, Evgeny V. Rebrov, Muhammad Naeem Ashiq, Shahzad Naseemd, M.U. Rana, Structural, infrared, magnetic and microwave absorption properties of rare earth doped X-type hexagonal nanoferrites, J. Alloys Compd. 570 (2013) 7–13.

[39] R. Rajesh Kanna, N. Lenin, K. Sakthipandi, M. Sivabharathy, Impact of lanthanum on structural, optical, dielectric and magnetic properties of $Mn_{1-x}Cu_xFe_{1.85}La_{0.15}O_4$ spinel nanoferrites, Ceram. Int. 43 (2017) 15868–15879.
[40] P.U. Aparna, N.K. Divya, P.P. Pradyumnan, Structural and dielectric studies Of Gd doped ZnO nanocrystals at room temperature, J. Mater. Sci. Chem. Eng. 4 (2016) 79–88.
[41] M.T. Rahman, M. Vargas, C.V. Ramana, Structural characteristics, electrical conduction and dielectric properties of gadolinium substituted cobalt ferrite, J. Alloys Compd. 617 (2014) 547–562.
[42] V. Pal, R.K. Dwivedi, Effect of rare earth substitution on the structural, microstructure and dielectric properties of lead free BNT ceramics, Adv. Mater. Res. 585 (2012) 200–204.
[43] Zhan-Guo Liu, Jia-Hu Ouyang, Yu Zhou, Xiao-Liang Xia, Effect of Sm substitution for Gd on the electrical conductivity of fluorite-type $Gd_2Zr_2O_7$, J. Power Sources 185 (2008) 876–880.
[44] K. Oikawa, T. Kamiyama, T. Hashimoto, Y. Shimojyo, Y. Morii, Structural phase transition of orthorhombic $LaCrO_3$ studied by neutron powder diffraction, J. Solid State Chem. 154 (2000) 524–529.
[45] T. Hashimoto, Analysis of crystal structure and phase transition of $LaCrO_3$ by various diffraction measurements, Solid State Ionics 132 (2000) 183–190.
[46] H. Hayashi, M. Watanabe, H. Inaba, Measurement of thermal expansion coefficient of $LaCrO_3$, Thermochim. Acta 359 (2000) 77–85.
[47] Michael W. Lufaso, Samuel J. Mugavero, William R. Gemmill, Y. Lee, Thomas Vogt, Hans-Cord ZurLoye, Pressure-and temperature- dependent x-ray diffraction studies of $NdCrO_3$, J. Alloys Compd. 433 (2007) 91–96.
[48] S. Sankarrajan, K. Sakthipandi, V. Rajendran, Temperature-dependent sound velocities, attenuation and elastic moduli anomalies in $Pr_{1-x}Sr_xMnO_3$ perovskite manganite materials at $0.28 \leq X \leq 0.41$, Phase Transitions 85 (2012) 427–443.